Supporting Information

Extracting Kinetics and Thermodynamics of Molecules without Heavy Atoms via Time-Resolved Solvent Scattering Signals

Key Young Oang,[1] Sungjun Park,[2,3] Jiwon Moon,[4] Eunji Park,[4] Hyun Kyung Lee,[5] Tokushi Sato,[6] Shunsuke Nozawa,[7] Shin-ichi Adachi,[7,8] Joonghan Kim,[4] Jeongho Kim,[9] Jeong-Hun Sohn,[*,5] and Hyotcherl Ihee[*,2,3]

[1]Radiation Center for Ultrafast Science, Korea Atomic Energy Research Institute (KAERI), Daejeon 34057, Republic of Korea

[2]Department of Chemistry and KI for BioCentury, Korea Advanced Institute of Science and Technology (KAIST), Daejeon 34141, Republic of Korea

[3]Center for Advanced Reaction Dynamics, Institute for Basic Science (IBS), Daejeon 34141, Republic of Korea

[4]Department of Chemistry, The Catholic University of Korea, Bucheon 14662, Republic of Korea

[5]Department of Chemistry, College of Natural Sciences, Chungnam National University, Daejeon 34134, Republic of Korea

[6]European XFEL, Holzkoppel 4, 22869 Schenefeld, Germany

[7]Institute of Materials Structure Science, High Energy Accelerator Research Organization, 1-1 Oho, Tsukuba, Ibaraki 305-0801, Japan

[8]Department of Materials Structure Science, School of High Energy Accelerator Science, the Graduate University for Advanced Studies, 1-1 Oho, Tsukuba, Ibaraki 305-0801, Japan

[9]Department of Chemistry, Inha University, 100 Inha-ro, Michuhol-gu, Incheon 22212, Republic of Korea

[*]Corresponding author: hyotcherl.ihee@kaist.ac.kr; sohnjh@cnu.ac.kr

Sample preparation. 36.5 g of HPDP was synthesized from 1-(4-hydroxyphenyl)ethanone in five steps following the literature procedures.[1]

TRXL data collection. TRXL measurement was performed at the NW14A beamline of KEK by following the experimental protocol described in our previous publications.[2,3] Third-harmonic generation of 800 nm output pulses from an amplified Ti:sapphire laser system provided 150 fs pulses at the center wavelength of 267 nm. The laser beam was focused by a lens to a spot of 300-μm diameter, where the laser beam was overlapped with the x-ray beam with a crossing angle of 10°. At the sample, the pulse energy was approximately 35 μJ, which yielded the fluence of about 0.5 mJ mm^{-2}. The laser pulses were synchronized with x-ray pulses from the synchrotron using an active feedback control loop that adjusts the laser oscillator cavity length, and the relative time delay between the laser and x-ray pulses was controlled electronically. Time-delayed x-ray pulses were selected by using a synchronized mechanical chopper. A multilayer optic coated with depth-graded Ru/C layers (d = 40 Å, NTT Advanced Technology) produced a Gaussian-type x-ray spectrum with center energy of 15.5 keV and a ~5% energy bandwidth. The x-ray beam was focused on a spot of 200-μm diameter at the sample position. The scattering patterns generated by x-ray pulses of 100-ps (full-width at half-maximum) duration were measured with an area detector (MarCCD165, Mar USA) with a sample-to-detector distance of 41 mm. We used *p*-hydroxyphenacyl diethyl phosphate (HPDP) dissolved in H_2O/MeCN co-solvent (2:1, v/v). The sample solution of 20-mM concentration was circulated through a sapphire nozzle with a 300-μm-thick aperture. The sample flow velocity was set to be over 3 m/s to supply a fresh sample for every pair of laser and x-ray pulses. The sample in the reservoir was replaced with a fresh one whenever the sample failed to produce the transient signal at 100 ps. Furthermore, even if the transient signal at 100 ps did not change, the sample in the reservoir was replaced with fresh one regularly (every 2 hours of measurement) to ensure the delivery of fresh samples. The time resolution of our TRXL experiment was 100 ps, which was limited by the duration of the x-ray pulses. The laser-off images were acquired with the x-ray pulse arriving 3 ns earlier than the laser pulse (that is, –3 ns time delay), to eliminate the contribution of the (unexcited) ground-state reactants. These laser-off images were used as a reference for calculating the time-resolved difference x-ray scattering patterns. To achieve a signal-to-noise ratio high enough for data analysis, more than 200 images were acquired and averaged at each time delay. The scattering curves were

measured at the following time delays: –3 ns, –200 ps, 100 ps, 133 ps, 178 ps, 237 ps, 316 ps, 422 ps, 562 ps, 750 ps, 1 ns, 1.78 ns, 3.16 ns, and 10 ns. The scattering signals arising from the heating of H_2O/MeCN co-solvent induced by the vibrational cooling process were also measured using an 80-mM $FeCl_3$ solution with the same experimental conditions.

SVD analysis. In order to determine how many structurally distinguishable transient solute species are involved in the reaction, we apply the singular value decomposition (SVD) analysis[4] to the TRXL data. From the experimental scattering curves measured at various time delays, we can build an $n_q \times n_t$ matrix **A**, where n_q is the number of q points in the scattering curve at a given time-delay point and n_t is the number of time-delay points. The matrix **A** can be decomposed while satisfying the relationship of $\mathbf{A} = \mathbf{USV}^{\mathrm{T}}$, where **U** is an $n_q \times n_t$ matrix whose columns are called left singular vectors (LSVs) (i.e., time-independent q spectra) of **A**, **V** is an $n_t \times n_t$ matrix whose columns are called right singular vectors (RSVs) (i.e., amplitude changes of **U** as time evolves) of **A**, and **S** is an $n_t \times n_t$ diagonal matrix whose diagonal elements are called singular values of **A** and can possess only non-negative values. The matrices **U** and **V** have the properties of $\mathbf{U}^{\mathrm{T}}\mathbf{U} = \mathbf{I}_{nt}$ and $\mathbf{V}^{\mathrm{T}}\mathbf{V} = \mathbf{I}_{nt}$, respectively, where $\mathbf{I}_{nt}$ is the identity matrix. Since the diagonal elements (i.e., singular values) of **S**, which represent the weight of LSVs and RSVs, are ordered so that $s_1 \geq s_2 \geq \cdots \geq s_n \geq 0$, LSVs and RSVs on more left are supposed to have a larger contribution to the TRXL data. In this manner, we can extract the time-independent scattering intensity components from the LSVs and the time evolution of their amplitudes from the RSVs. Here we note that, in order to constrain the LSVs to be perfectly identical for the TRXL data of HPDP and that of $FeCl_3$, we performed SVD analysis by treating two sets of TRXL data simultaneously and thus the size of matrix **A** was set to be $n_q \times 2n_t$.

MD simulations. MD simulations were performed using the program MOLDY.[5] The TIPS2 water model[6] and Edwards' MeCN model[7] were used and the Lennard–Jones parameters for the co-solvent were modified. For the simulation of the solvent response, we used 1,110 rigid water molecules and 190 rigid acetonitrile molecules in a cubic box with a side length of ~50 Å, which was large enough to avoid parasitic oscillations in the differentials at low q. The radial distribution functions were calculated up to 50 Å in steps of 0.02 Å and used for the calculation of the scattering intensity. By considering the Longaker–Litvak time[8] of this study

(τ_L = ~100 ns), we simulated only two thermodynamic conditions (C1: T_1 = 300 K, ρ_1 = 929 kg m^{-3}; C2: T_2 = 330 K, ρ_2 = 929 kg m^{-3}). Taking the difference between the scattering intensity of the system in condition C1, S(C1), from that in C2, S(C2), and further dividing the difference by the temperature change (in this case, 30 K), gives the changes in the scattering intensity due to temperature change at "constant density", $q(\partial S/\partial T)_\rho$. In addition, the blurring of the scattering intensity (S) due to the polychromaticity was properly corrected by the polychromatic correction.[9]

Solvent response. In the solution phase, the solute species (molecules, ions, or atoms of interest) are dissolved in a solvent that, in most cases, outnumbers the solute. Since x-ray scatters and diffracts from all atom–atom pairs, difference scattering intensity of TRXL, $\Delta S(q,t)$, has three principal contributions:[8–11] i) the solute-only term ($q\Delta S_{\text{solute}}(q,t)$) from the internal structure of the solute molecules, ii) the solute–solvent cross term ($q\Delta S_{\text{solute-solvent}}(q,t)$) from solute–solvent atomic pairs, and iii) the solvent-only term ($q\Delta S_{\text{solvent}}(q,t)$) from the bulk solvent that, in general, dominates the others, and $q\Delta S(q,t)$ can be expressed by Eqn. (1):

$$\begin{aligned} q\Delta S(q,t) &= q\left[\Delta S_{\text{solute}}(q,t) + \Delta S_{\text{solute-solvent}}(q,t)\right] + q\Delta S_{\text{solvent}}(q,t) \\ &= q\Delta S_{\text{solute related}}(q,t) + q\Delta S_{\text{solvent}}(q,t) \end{aligned} \tag{1}$$

where R is the ratio of solvent to solute molecules, k represents the chemical species (reactant, intermediates, and products), $c_k(t)$ is the fraction of species k at time t after photoexcitation, and $qS_k(q)$ and $qS_g(q)$ are the scattering intensities of species k and that of species in the ground state, respectively.

For solute molecules that lack heavy-atom constituents, $q\Delta S(q,t)$ in Eqn. (1) can be simplified by Eqn. (2):

$$q\Delta S(q,t) \approx q\Delta S_{\text{solvent}}(q,t) \tag{2}$$

In general, the temporal evolution of the solvent-only term at any time can be fully described as a linear combination of two components pertaining to the photo-induced changes in two independent thermodynamic variables, temperature (T) and density (ρ) of solvent, as shown in Eqn. (3):

$$q\Delta S(q,t) \approx q\Delta S_{\text{solvent}}(q,t) = q\left(\frac{\partial S(q)}{\partial T}\right)_{\rho} \Delta T(t) + q\left(\frac{\partial S(q)}{\partial \rho}\right)_{T} \Delta\rho(t) \tag{3}$$

where $q(\partial S/\partial T)_{\rho}$ and $q(\partial S/\partial \rho)_{T}$ are the changes in $q\Delta S(q,t)$ due to temperature change at a constant density and density change at a constant temperature, respectively. Especially, it is known that for time delays sufficiently short ($t \ll \tau_{\text{L}} = L/c$), where τ_{L} is the so-called Longaker–Litvak time, L is the radius of the laser spot, and c is the speed of sound in the liquid, the solvent is heated at constant density ($\Delta\rho(t \ll \tau_{\text{L}}) = 0$).[8] In other words, thermal expansion of the solvent does not set in immediately after the heat input, but is delayed as perturbations in a liquid cannot propagate faster than sound waves. In this study, $c_{\text{H2O/MeCN}} = \sim c_{\text{H2O}} = \sim$1481 m/s and $L = \sim$150 μm, which leads to $\tau_{\text{L}} = \sim$100 ns, and thus, for $q\Delta S(q,t)$ measured at sufficiently shorter time delays (from 100 ps to 10 ns) than τ_{L} (~100 ns), $q\Delta S(q,t)$ can be further simplified by Eqn. (4):

$$q\Delta S(q,t) \approx q\left(\frac{\partial S(q)}{\partial T}\right)_{\rho} \Delta T(t) \tag{4}$$

Absolute scaling factor ($\alpha\beta$) and temperature change of the solvent ($\Delta T(t)$). We calculated the absolute scaling factor ($\alpha\beta$) between the experimental TRXL data, $q\Delta S_{\text{exp}}(q,t)$, and the theoretical ones obtained from the MD simulations, $\Delta S_{\text{MD}}(q,t)$, by using the averaged experimental scattering curve of laser-off images and the theoretical scattering curve of the co-solvent calculated by MOLDY.[5] First, we calculated the scaling factor (α) by comparing the averaged experimental scattering curve of laser-off images with the theoretical scattering curve of the co-solvent:

$$\begin{aligned} \alpha qS(q,t_{\mathrm{ref}}) &\approx qS_{\mathrm{MD}}(q,T_1,\rho) \\ \alpha qS(q,t\quad) &\approx qS_{\mathrm{MD}}(q,T_2,\rho) \end{aligned} \tag{5}$$

Because the difference scattering curves at all time delays were normalized by the normalization factor (β) that is identical to the area under the averaged scattering curve of laser-off images within the high-q part of the spectrum, where the intensity at the particular q interval is constant regardless of time delay, the following relationship holds:

$$q\Delta S(q,t) = \frac{qS(q,t)}{\beta_1} - \frac{qS(q,t_{\mathrm{ref}})}{\beta_2} \approx \frac{q\left[S(q,t) - S(q,t_{\mathrm{ref}})\right]}{\beta} \tag{6}$$

By combining Eqns. (5) and (6), the following relationship also holds:

$$\Delta T(t) \approx \alpha\beta\Delta S(q,t) \Big/ \left(\frac{\partial S(q)}{\partial T}\right)_{\rho} \tag{7}$$

Fitting analysis of hydrodynamics. By minimizing the discrepancy quantified by the χ^2 value between the experimentally obtained temperature changes of the solvent ($\Delta T_{\mathrm{exp}}(t)$) and the theoretically calculated ones ($\Delta T_{\mathrm{thy}}(t)$), we optimized the energies of the chemical species involved in the photochemical reaction of HPDP:

$$\chi^2 = \sum_i \left(\frac{\Delta T_{\mathrm{exp}}(t_i) - \Delta T_{\mathrm{thy}}(t_i)}{\sigma_{\mathrm{exp}}(t_i)} \right)^2 = \sum_i \left(\frac{\Delta T_{\mathrm{exp}}(t_i) - \Delta Q_{\mathrm{thy}}(t_i)/C_{\mathrm{V,m}}}{\sigma_{\mathrm{exp}}(t_i)} \right)^2 \tag{8}$$

where $\Delta Q_{thy}(t)$ is the heat released per mole of solvent molecules (in J/mol), $C_{V,m}$ is the molar heat capacity of the co-solvent at constant volume (in J/mol/K). The calculation of the heat released, $\Delta Q_{thy}(t)$, to the solvent is straightforward once the population of the different states, $c_k(t)$, are known. $\Delta Q_{thy}(t)$ can be calculated using the following equation.

$$\Delta Q_{thy}(t) = \frac{N_A}{R} f_{rxn} \left\{ (1 - f_{vib}) \left[h\upsilon \sum_k c_k(0) - \sum_k \Delta H_k c_k(t) \right] + h\upsilon f_{vib} \left[1 - \exp\left(-\frac{t}{\tau_{vib}} \right) \right] \right\} \quad (9)$$

$k = \{\text{chemical species 1, chemical species 2, chemical species 3}\}$

In Eqn. (9), ΔH_k is the enthalpy of the state k (in J/mol) relative to that of HPDP (we set H_{HPDP} = 0 J/mol), $h\upsilon$ is the energy of photons per mole (in J/mol), R is the ratio between solvent molecules and solute molecules, N_A is the Avogadro number, and f_{rxn} is the unitless fractional concentration of HPDP molecules undergoing the reactions of interest, that is, the photo-Favorskii rearrangement and the vibrational cooling process. The last term (f_{vib}), also unitless, was inserted to take into account the very fast recovery of the ground state, HPDP, via the vibrational cooling process. Based on the results of the SVD analysis, the subsequent fitting of the 1st RSV with a sum of two exponentials, and the previously proposed kinetic frameworks in the literature (shown in Figure S1), we used a simple sequential kinetic model with three chemical species (A, B, and C) and two relaxation times (230 ± 20 ps for A→B and 1.7 ± 0.6 ns for B→C) for the calculation of the population changes of the different states, $c_k(t)$. As a result of the fitting analysis of hydrodynamics, we optimized f_{rxn} (38.3 ± 1.2%) and f_{vib} (4.6 ± 0.4%) as well as ΔH_k's of A (249 ± 10 kJ/mol), B (178 ± 14 kJ/mol), and C (160 ± 13 kJ/mol). The errors here account for only random errors, not systematic errors, and the seemingly small errors reflect only precision, not accuracy.

A summary of previous studies of the photo-induced reaction of HPDP in H_2O/MeCN. Figure S1 summarizes the representative reaction mechanisms of the photochemical reaction of HPDP in H_2O/MeCN proposed in previous time-resolved spectroscopic and theoretical studies.[1,12–15] Here we note that, according to the previous studies,[1,12–15] irradiation with ultraviolet light excites the HPDP molecule from its ground state to the singlet excited state,

which within 4 ps undergoes intersystem crossing to reach the triplet excited state (T_1), and thus Figure S1 only shows the reaction steps occurring later than the formation of T_1. The steady-state absorption spectrum of HPDP in H_2O/MeCN is shown in Figure S2. As can be seen in Figure S1, the reaction mechanism and the reaction intermediates of the photochemical reaction of HPDP still remain controversial. Phillips and co-workers[1] investigated the decay dynamics of T_1 of the deprotection reaction and the formation dynamics of the rearrangement product (HPAA) for two types of photocaged molecules with different leaving groups, HPDP and *p*-hydroxyphenacyl diphenyl phosphate (HPPP) in H_2O/MeCN (1:1, v/v). Transient absorption (TA) and time-resolved resonance Raman (TR^3) spectroscopy were used to monitor the decay dynamics of T_1 and the formation dynamics of HPAA, respectively. The discrepancies between the time scales of the T_1 decay (350 ± 20 ps and 150 ± 20 ps in cases of HPDP and HPPP, respectively) and the HPAA formation (470 ± 40 ps and 600 ± 40 ps in cases of HPDP and HPPP, respectively) indicate that there are additional reaction steps between the deprotection and rearrangement reactions. In addition, for HPDP, the T_1 decay is slower and the HPAA formation is faster than for HPPP. Such differences in the dynamics of T_1 decay and HPAA formation for HPDP and HPPP are attributed to the larger pK_a value and the smaller size, respectively, of the diethyl phosphate anion in HPDP than those of the diphenyl phosphate anion in HPPP. Furthermore, it was found that the rate of deprotection sensitively changes with the fraction of water in the water/MeCN co-solvent (that is, the higher the fraction of water, the faster T_1 decay), indicating the participation of water in the deprotection reaction. In contrast, the rate of rearrangement does not depend on the fraction of water, suggesting that the local solvation environment around the solute is not influenced by the presence of water on the time scale of the rearrangement reaction. Based on the observed dependence of reaction dynamics on the leaving group and the solvent composition, ^{3}CIP was suggested as an intermediate formed between the deprotection and rearrangement reactions (see the Proposed mechanism 1 in Figure S1).

Later, for the solution sample of HPDP in more aqueous H_2O/MeCN (7:1, v/v), Givens and co-workers[13] used TA spectroscopy to observe the primary photoproduct that is formed from T_1 and exhibits very weak TA signal. In the H_2O/MeCN co-solvent with the high fraction of water, the T_1 decay (100 ± 10 ps time constant) is much faster than the decay of the primary photoproduct (~600 ps time constant), thus giving enough time to observe the primary photoproduct at a high concentration. By comparing the positions and shapes of the absorption

bands of the primary photoproduct with those of the phenoxy radical, they assigned the primary photoproduct to ^{3}AP rather than ^{3}CIP, which was proposed previously by Phillips and co-workers[1] as the intermediate species between T_1 and HPAA. In addition, *p*-hydroxybenzyl alcohol (^{1}HBA), a side product of the photochemical reaction of HPDP in the H_2O/MeCN co-solvent with a low fraction (< 10 %) of water, was also observed. It was predicted that ^{1}HBA is formed through the intersystem crossing of ^{3}AP, immediate cyclization of ^{1}AP, decarbonylation of ^{1}SK, and subsequent hydration of *p*-quinone methide (^{1}QM). The yield of ^{1}HBA was observed to decrease and, at the same time, that of HPAA was observed to increase with the increase of the fraction of water in the water/MeCN co-solvent. Thus, they suggested that a putative intermediate, ^{1}SK, must be a real intermediate but is not directly observed because it is rapidly converted to HPAA, even in the co-solvent with a high fraction of water (see the Proposed mechanism 2 in Figure S1).

Later, Phillips and co-workers[14] studied the photo-Favorskii rearrangement of HPDP in deuterated co-solvent, D_2O/CD_3CN (1:1, v/v), using time-resolved infrared (TRIR) and TR^3 spectroscopy. In the deuterated co-solvent, the overall kinetics of the reaction are supposed to be decelerated, which is so-called the solvent kinetic isotope effect. In that study, it was revealed that ^{3}CIP is rapidly formed via the photo-induced deprotection of T_1 within 100 ps, that is, even faster than the T_1 decay (350 ps) in H_2O/MeCN (1:1, v/v) observed in their earlier study.[1] This observation contradicts the prediction that the T_1 decay will be slower in the deuterated solvent. In addition, according to their DFT calculations, the solvation efficiently lowers the energy barrier between T_1 and ^{3}CIP, leading to the ultrafast deprotection of T_1. Based on these results, they changed their own assignment of the early intermediate T_1 in their earlier study[1] to ^{3}CIP. In addition, another intermediate species was observed to be formed from ^{3}CIP before the formation of HPAA. To identify that extra intermediate species, two reaction pathways were considered in that work (see P1 and P2 of the Proposed mechanism 3 in Figure S1).[14] In one candidate reaction pathway (P1), as Givens and co-workers suggested in their previous study,[13] the additional intermediate was assigned to ^{3}AP, which sequentially transforms to ^{1}SK, 1,1'-di-hydroxyl-SK (^{1}SK'),[12,14] and HPAA. In another candidate pathway (P2), the additional intermediate was assigned to a triplet cation species (^{3}CS), which sequentially transforms into ^{3}HPAAH$^+$ and HPAA. However, the results of their DFT calculations suggested that the energy barriers between ^{1}SK and ^{1}SK' (134 kJ/mol) and between

^{1}SK' and HPAA (96 kJ/mol) in P1 and the energy barrier between ^{3}CIP and ^{3}CS in P2 (188 kJ/mol) are too large to explain the rapid formation of HPAA (~470 ps).[1]

Quantum yield of the photo-Favorskii rearrangement. We calculated the quantum yield of the photo-Favorskii rearrangement using the optimized values of f_{rxn} and f_{vib} obtained from the fitting analysis of hydrodynamics. The focal spot of the laser pulse was circular with a radius of 0.15 mm with an energy density of 0.5 mJ/mm^2 at 267 nm, giving 4.7×10^{13} photons/pulse. In detail, [$\pi \times (0.15\ \text{mm})^2 \times (0.5\times10^{-3}$ J/mm^2/pulse)] / [(6.626×10^{-34} m^{2}kg/s $\times$ 3×10^8 m/s) / (267×10^{-9} m)] = 4.747×10^{13} photons/pulse. In the interaction volume of 2.3×10^{-3} mm^3, 2.78×10^{13} HPDP molecules are contained, which is 1.7 times smaller than the number of photons in the laser pulse. Since the extinction coefficient of HPDP is very high (15.1 mM^{-1} cm^{-1}) at 267 nm, the optical density is 0.99 for the 0.03-mm penetration depth and the 20-mM sample-solution concentration. In detail, the sample depth for the optical density of 0.99 is 0.99 / [(15,136 M^{-1} cm^{-1}) $\times$ (0.02 M)] $\times$ 10 = 0.0327 mm. Thus, the number of HPDP molecules in the interaction volume is [$\pi \times (0.15\ \text{mm})^2 \times 0.0327$ mm] $\times$ [$0.02 \times 6.02\times10^{23}$ / (100 mm)^3] = 2.78×10^{13} HPDP molecules. Thus, it turned out that the experimental condition regarding the fluence of the pump laser was enough to excite all the HPDP molecules. As a result, the quantum yield ($\boldsymbol{\Phi}_1$) of photo-Favorskii rearrangement we obtained is:

$$\Phi_1 = \frac{f_{rxn} \times (1 - f_{vib})}{\text{probability of HPDP molecules photoexcited}} = \frac{(0.383 \pm 0.012) \times (0.954 \pm 0.004)}{1.0} = 0.365 \pm 0.013 \qquad (10)$$

Similarly, the quantum yield ($\boldsymbol{\Phi}_2$) of the vibrational cooling we obtained is:

$$\Phi_2 = \frac{f_{rxn} \times f_{vib}}{\text{probability of HPDP molecules photoexcited}} = \frac{(0.383 \pm 0.012) \times (0.046 \pm 0.004)}{1.0} = 0.018 \pm 0.002 \qquad (11)$$

Similarly, the quantum yield ($\boldsymbol{\Phi}_3$) of the remainder, which is likely to rapidly relax to the ground state without heat release into the surrounding solvent via fluorescence emission from the initially populated singlet excited states, is:

$$\Phi_3 = 1 - \Phi_1 - \Phi_2 = 1 - (0.365 \pm 0.013) - (0.018 \pm 0.002) = 0.617 \pm 0.015 \quad (11)$$

The errors in $\mathbf{\Phi}_1$, $\mathbf{\Phi}_2$, and $\mathbf{\Phi}_3$ account for only random errors, not systematic errors, and the seemingly small errors reflect only precision, not accuracy. The obtained $\mathbf{\Phi}_2$ is quite a small number. To check its reliability, we forced the value of f_{vib} to be fixed at zero and checked the fitting quality. As a result, as much as the contribution of vibrational cooling disappeared, f_{rxn} (0.383→0.398), ΔH_k's of A (249 kJ/mol→254 kJ/mol), B (178 kJ/mol→179 kJ/mol), and C (160 kJ/mol→163 kJ/mol) tended to increase slightly to compensate the fit, but the χ^2 value when $f_{vib} = 0$ showed a larger value by about 4%. After fitting with the f_{vib} value fixed at zero, we confirmed that if the f_{vib} value was set as a free variable and fitted again, optimized values of f_{vib} as well as f_{rxn}, ΔH_k's of A, B, and C returned to the original values we are reporting in this work.

DFT calculations. Geometry optimizations and subsequent harmonic vibrational frequency calculations were performed using density functional theory (DFT) with ωB97XD functional. The 6-311G(d,p) basis sets were used in the DFT calculations. All molecular structures were fully optimized without any symmetry constraints. The solvent (water) effect was modeled with the integral equation formalism version of the polarizable continuum model (IEFPCM). We considered the solute species with eight water molecules explicitly solvating the solute molecules. The good agreement between ΔH_{DFT}'s of ^{3}CIP and ^{3}AP with ΔH_{exp} of the first two species suggests that eight explicit water molecules used for the DFT calculations with ωB97XD functional are sufficient to account for the solvation effect in the reaction steps from HPDP to ^{1}SK where no water molecule directly participates in (see the main text for details). On the other hand, for the reaction from ^{1}SK to HPAA, one water molecule directly reacts with ^{1}SK, resulting in the breaking and formation of covalent bonds (solvolytic reaction). In detail, it was theoretically predicted that a water molecule attacks the C atom of a C=O group in the ^{1}SK species to form a ^{1}SK' species, and an H atom of the hydroxyl group in the ^{1}SK' species is transferred to the *para*-O atom with the assistance by the solvating water molecules to generate HPAA.[12,14] Although HPAA is expected to have a lower ΔH_{DFT} than ^{1}SK, the hydrogen-bonding network of water molecules around ^{1}SK and HPAA molecules needs to be properly

described to calculate their ΔH_{DFT}'s accurately. As an example, we optimized the structures of the solute molecules (that is, ^{1}SK and HPAA) solvated by water molecules and calculated the difference in ΔH_{DFT}, $\Delta\Delta H_{DFT}$, between ^{1}SK and HPAA. Then, we repeated the geometry optimization while adding two extra water molecules to the optimized solvated structures, starting with eight water molecules and up to eighteen water molecules, as shown in Figure S7. We also tried to optimize the structures of the solute molecules solvated by more than twenty water molecules but the optimization failed, probably due to the existence of multiple conformations with many solvent molecules around. As shown in Figure S7, $\Delta\Delta H_{DFT}$ between ^{1}SK and HPAA varies sensitively with the change of solvating water molecules, probably because ΔH_{DFT}'s of ^{1}SK and HPAA depend strongly on the initial positions of the newly added water molecules, especially when many water molecules are present.

We also used other DFT methods, including B3LYP, CAM-B3LYP, M06-2X, MN12-SX, and MN15, to compare the calculated results with those of ωB97XD. The calculated results are summarized in Table S2. In addition, for S_0, T_1, ^{3}CIP, and ^{3}AP, all DFT methods (ωB97XD, B3LYP, CAM-B3LYP, M06-2X, MN12-SX, and MN15) were used to optimize their molecular structures with thirteen explicit water molecules, instead of eight, to investigate the dependence on the number of explicit water molecules used to describe the solvent effect. The calculated results are also listed in Table S2. The geometry optimizations of ^{3}CIP using all DFT methods with thirteen explicit water molecules were unsuccessful and the optimized structure converged to the ^{3}AP state, suggesting that ^{3}CIP may not be stable. All calculations were performed using the Gaussian09 and 16 programs.[16]

Table S1. Comparison with previous studies of the photo-induced reaction of HPDP in H_2O/MeCN

	Proposed mechanism 1[a]	**Proposed mechanism 2**[b]	**Proposed mechanism 3**[c]	**This work**
Solvent	H_2O/MeCN (1:1, v/v)	H_2O/MeCN (7:1, v/v)	D_2O/CD_3CN (1:1, v/v)	H_2O/MeCN (2:1, v/v)
$T_1 \rightarrow {}^3CIP$	350 ± 20 ps	100 ± 10 ps	15 ± 9 ps	< 100 ps
$^3CIP \rightarrow {}^3AP$	470 ± 40 ps		1.2 ± 0.2 ns	230 ± 20 ps
$^3AP \rightarrow {}^1SK$		~600 ps	26 ± 5 ns	1.7 ± 0.6 ns
$^1SK \rightarrow {}^1SK'$				
$^1SK' \rightarrow$ HPAA				
Methods	TA & TR^3	TA	TRIR & TR^3	TRXL

[a]See the section "A summary of previous studies of the photo-induced reaction of HPDP in H_2O/MeCN" and Proposed mechanism 1 in Figure S1 for details.

[b]See the section "A summary of previous studies of the photo-induced reaction of HPDP in H_2O/MeCN" and Proposed mechanism 2 in Figure S1 for details.

[c]For the simplicity of Table S1, we only denote the chemical species of the P1 pathway in Table S1. See the section "A summary of previous studies of the photo-induced reaction of HPDP in H_2O/MeCN" and Proposed mechanism 3 in Figure S1 for details.

Table S2. Enthalpy changes (ΔH_{DFT}, in kJ/mol) of the S_0 and T_1 states of HPDP, intermediates, and HPAA calculated using various DFT methods with 6-311G(d,p). Eight explicit water molecules were used. Values in parentheses are ΔH_{DFT} of the S_0 and T_1 states of HPDP, and ^{3}AP with thirteen explicit water molecules.

	ωB97XD	B3LYP	CAM-B3LYP	M06-2X	MN12-SX	MN15
S_0	0 (0)	0 (0)	0 (0)	0 (0)	0 (0)	0 (0)
T_1	292 (250)	267 (233)	280 (244)	301 (256)	296 (260)	297 (256)
^{3}CIP	252	226	226	267	267	268
^{3}AP	165 (191)	143 (176)	148 (178)	181 (197)	184 (202)	184 (203)
^{3}CS	250	229	235	269	271	275
^{1}SK	140	115	128	136	158	146
HPAA	–126	–122	–136	–131	–118	–120

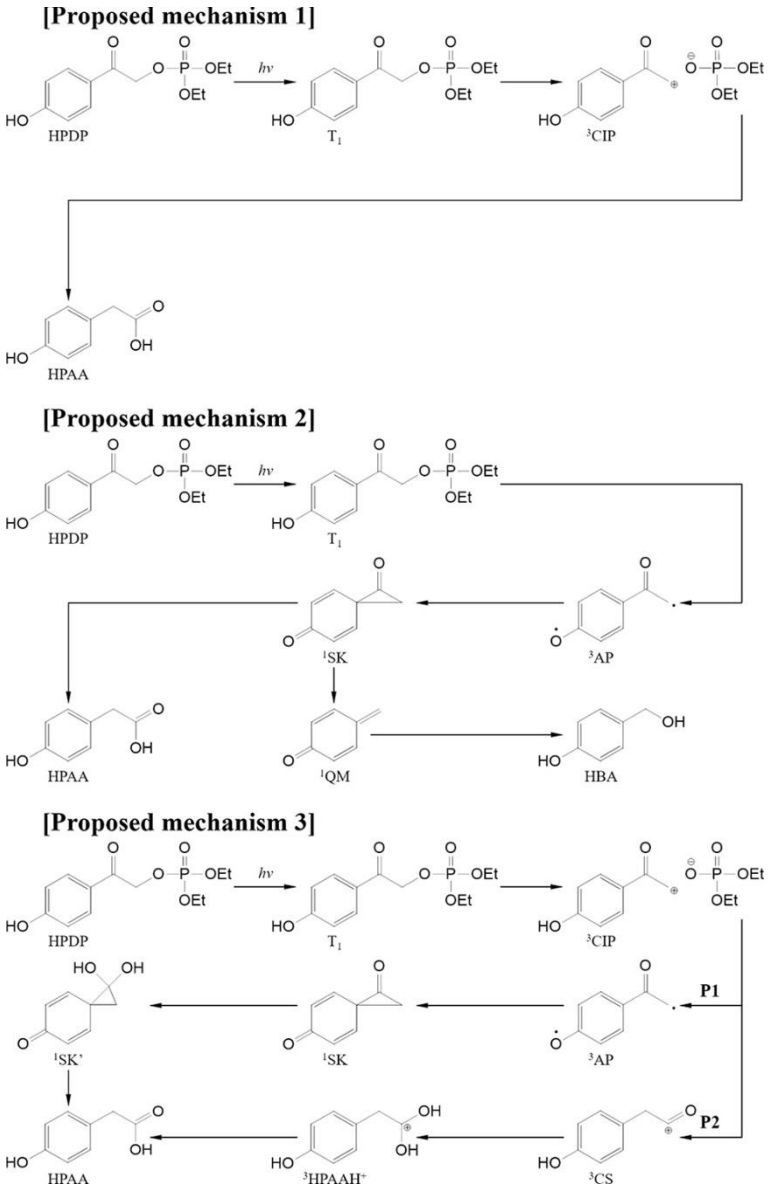

Figure S1. Three representative reaction mechanisms of the photochemical reaction of HPDP in H_2O/MeCN proposed in previous time-resolved spectroscopic and theoretical studies. See the main text and Table S1 for details.

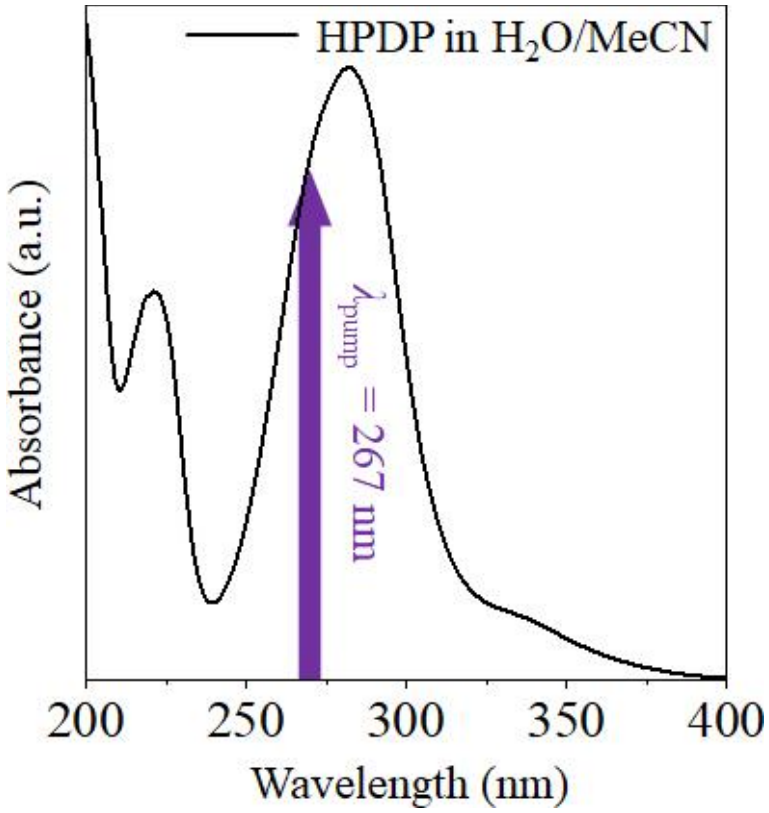

Figure S2. Steady-state absorption spectrum of HPDP (0.1 mM) in H_2O/MeCN (2:1, v/v).

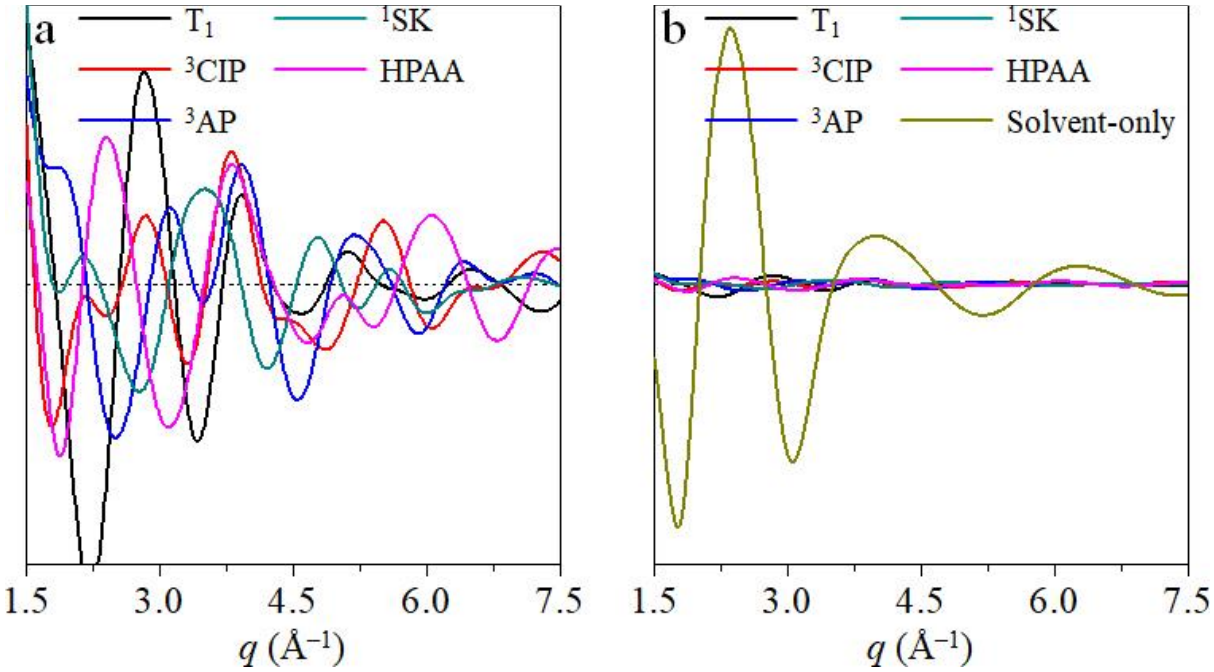

Figure S3. Comparison of the difference scattering intensities, $q\Delta S(q)$, from the solute molecules and solvent molecules. (a) Solute-only curves calculated for each candidate species (T_1, ^{3}CIP, ^{3}AP, ^{1}SK, and HPAA (S_0)). (b) Comparison of calculated solute-only scattering curves, $q\Delta S(q)$, and solvent-only one by considering the sample concentration (~20 mM). Because the scattering intensities from the solute molecules are negligibly small, and thus within our signal-to-noise ratio, the total scattering pattern of the solution sample can be expected to be essentially the same as the scattering from solvent alone.

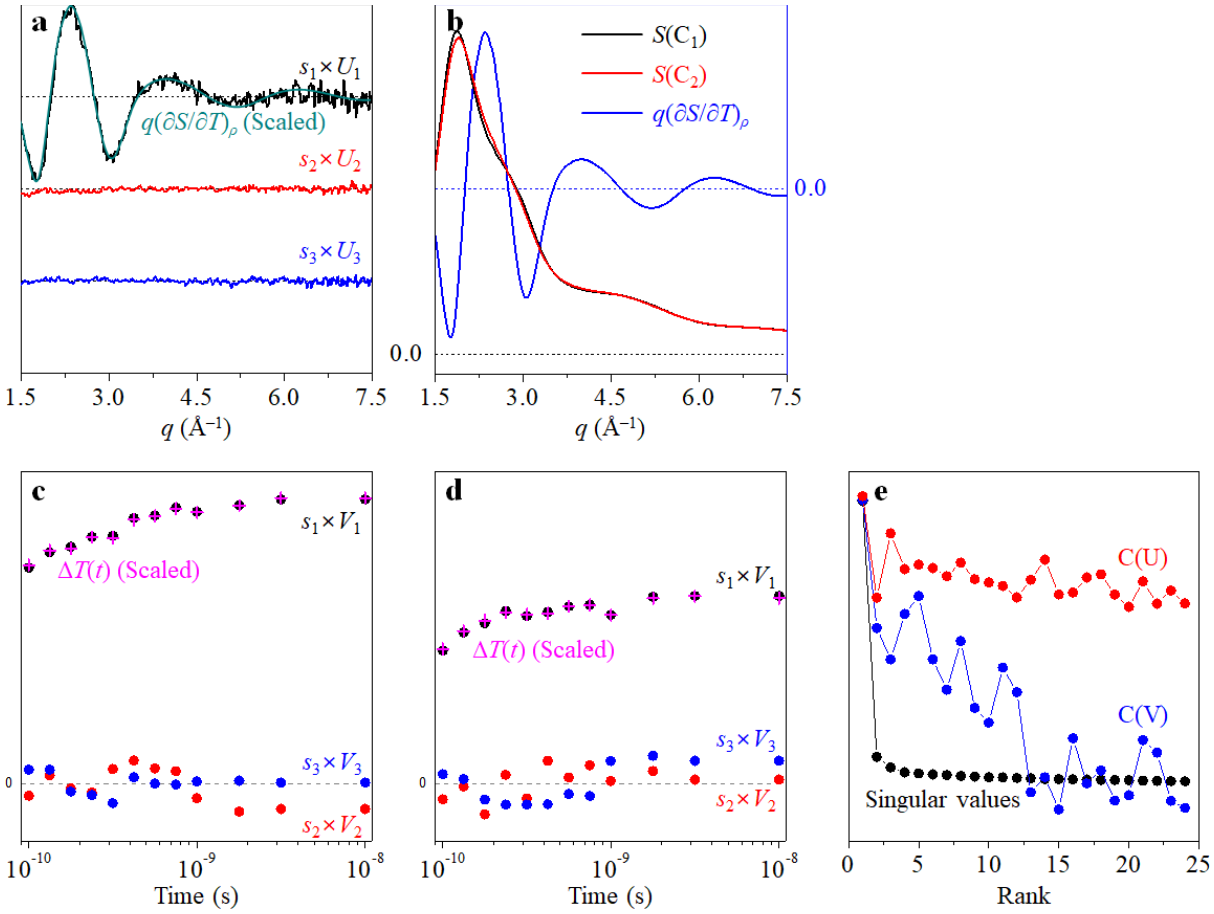

Figure S4. SVD analysis performed simultaneously for the TRXL data of HPDP and $FeCl_3$ and MD simulations. (a) The first three left singular vectors (LSVs) multiplied by singular values. Only the first LSV (black curve) has significant amplitude and agrees well with $q(\partial S/\partial T)_\rho$ calculated with the aid of MD simulations (dark cyan curve). (b) MD simulations of the solvent response for H_2O/MeCN co-solvent. Two thermodynamic conditions were simulated (C_1: T = 300 K, ρ = 929 kg/m^3; C_2: T = 330 K, ρ = 929 kg/m^3). By subtracting the scattering intensity, $S(C_2)$, of the system in condition C_2 (red curve) from the scattering intensity, $S(C_1)$, in C_1 (black curve) and dividing the difference by the temperature change, we obtained the change of scattering intensity change arising from the temperature change of bulk co-solvent at constant density ($(\partial S/\partial T)_\rho$). To magnify the scattering intensity at high angles, $(\partial S/\partial T)_\rho$ was multiplied by q to obtain $q(\partial S/\partial T)_\rho$ (blue curve). In addition, to take into account the effect of polychromatic x-ray used in the experiment, we applied the polychromatic correction to the calculated scattering curves. (c) The first three right singular vectors (RSVs) multiplied by singular values obtained from TRXL data of HPDP. $\Delta T(t)$ of the HPDP sample, which is shown in Figure S5 and also shown here for comparison (magenta crosses), coincides with the first RSV. (d) The first three right singular vectors (RSVs) multiplied by singular

values obtained from TRXL data of $FeCl_3$. $\Delta T(t)$ of the $FeCl_3$ sample, which is shown in Figure S5 and also shown here for comparison (magenta crosses), coincides with the first RSV. (e) Singular values (black solid circles), autocorrelations of LSVs (C(U), red solid circles), and autocorrelations of RSVs (C(V), blue solid circles).

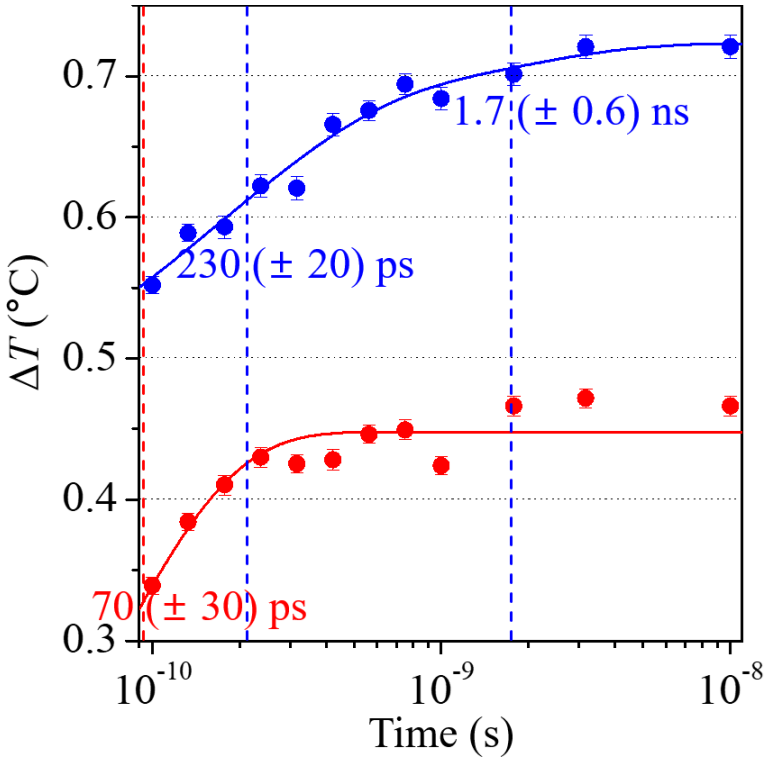

Figure S5. The changes in temperature over time ($\Delta T(t)$) obtained via TRXL of a solution containing HPDP and its control solution containing $FeCl_3$ and fits with relaxation times. Relaxation times associated with the photochemical reaction of HPDP were determined by fitting $\Delta T(t)$ of HPDP (blue circles) using a sum of two exponentials (blue curve). For $FeCl_3$, we assumed that $FeCl_3$ molecules release heat into the surrounding solvent only by vibrational cooling and thus fit $\Delta T(t)$ of $FeCl_3$ (red circles) using a single exponential (red curve). From the fitting, we obtained the relaxation times of 70 ± 30 ps for $FeCl_3$ (red vertical dashed line) and 230 ± 20 ps and 1.7 ± 0.6 ns for HPDP (blue vertical dashed lines).

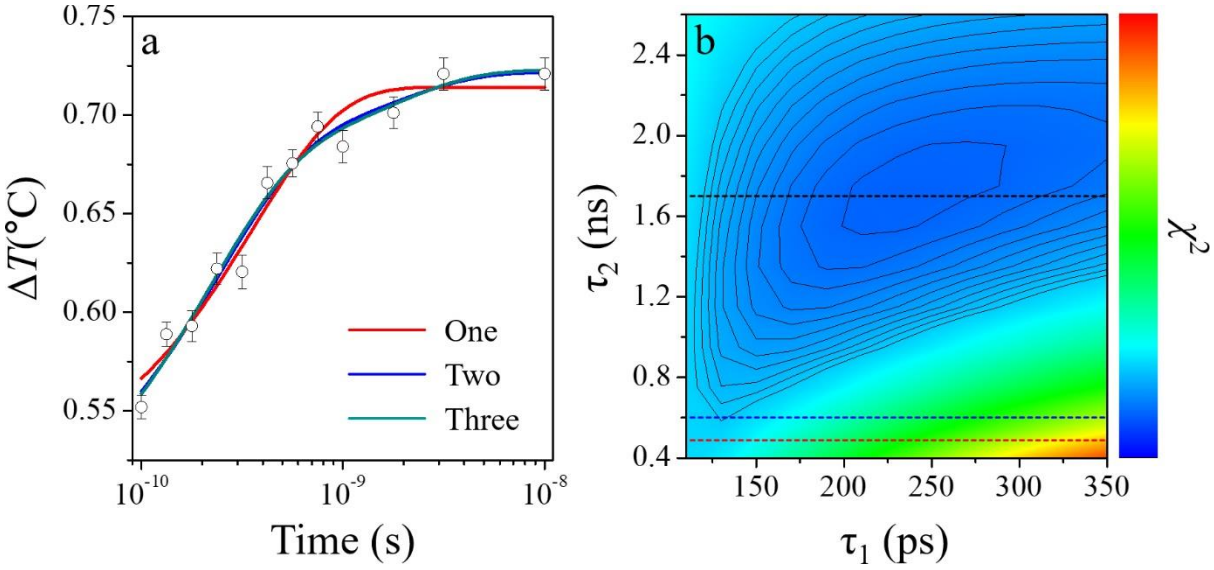

Figure S6. (a) Temperature changes of HPDP obtained from the TRXL experiment fitted with one (red curve), two (blue curve), and three (dark cyan curve) exponentials. The fit with one relaxation time produces a significantly worse match with the experimental data compared to the fit with two relaxation times. The use of three relaxation times does not result in improvement, suggesting that the data supports the use of only two relaxation times. (b) χ^2 values as a function of two relaxation times (τ_1 and τ_2) to demonstrate their statistical significance. The resulting figure visually illustrates the confidence level of the two relaxation times. Three horizontal dashed lines are drawn to indicate previously reported values for the second relaxation time (τ_2) associated with the formation of HPAA (470 ps (red dashed line) and 600 ps (blue dashed line))[1,13,15] and the value obtained in this work (1.7 ns (black dashed line)).

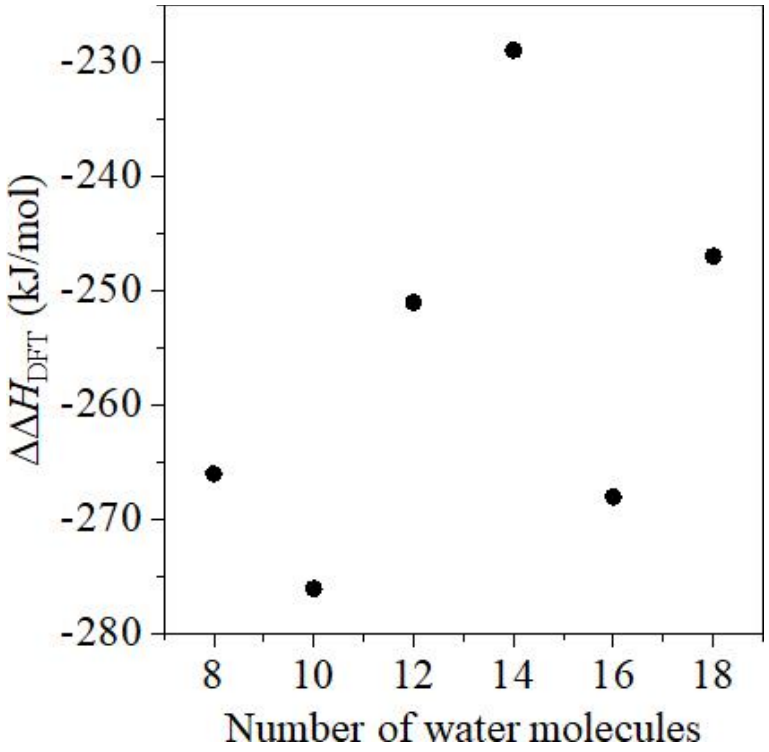

Figure S7. The difference in ΔH_{DFT}, $\Delta\Delta H_{DFT}$, between ^{1}SK and HPAA by varying the number of water molecules around the solute molecules (that is, HPAA and ^{1}SK). $\Delta\Delta H_{DFT}$ between ^{1}SK and HPAA varies sensitively with the change of solvating water molecules, probably because ΔH_{DFT}'s of ^{1}SK and HPAA depend strongly on the initial positions of the newly added water molecules, especially when many water molecules are present.

References

(1) Ma, C.; Kwok, W. M.; Chan, W. S.; Du, Y.; Kan, J. T. W.; Toy, P. H.; Phillips, D. L. Ultrafast time-resolved transient absorption and resonance Raman spectroscopy study of the photodeprotection and rearrangement reactions of *p*-hydroxyphenacyl caged phosphates. *J. Am. Chem. Soc.* **2006**, *128*, 2558–2570.

(2) Kim, K. H.; Lee, J. H.; Kim, J.; Nozawa, S.; Sato, T.; Tomita, A.; Ichiyanagi, K.; Ki, H.; Kim, J.; Adachi, S.; Ihee, H. Solvent-dependent molecular structure of ionic species directly measured by ultrafast x-ray solution scattering. *Phys. Rev. Lett.* **2013**, *110*, 165505.

(3) Park, S.; Choi, J.; Ki, H.; Kim, K. H.; Oang, K. Y.; Roh, H.; Kim, J.; Nozawa, S.; Sato, T.; Adachi, S.; Kim, J.; Ihee, H. Fate of transient isomer of CH_2I_2: Mechanism and origin of ionic photoproducts formation unveiled by time-resolved x-ray liquidography. *J. Chem. Phys.* **2019**, *150*, 224201.

(4) Oang, K. Y.; Yang, C.; Muniyappan, S.; Kim, J.; Ihee, H. SVD-aided pseudo principal-component analysis: A new method to speed up and improve determination of the optimum kinetic model from time-resolved data. *Struct. Dyn.* **2017**, *4*, 044013.

(5) Refson, K. Moldy: A portable molecular dynamics simulation program for serial and parallel computers. *Comput. Phys. Commun.* **2000**, *126*, 310–329.

(6) Jorgensen, W. L. Revised TIPS for simulations of liquid water and aqueous solutions. *J. Chem. Phys.* **1982**, *77*, 4156–4163.

(7) Edwards, D. M. F.; Madden, P. A.; McDonald, I. R. A computer simulation study of the dielectric properties of a model of methyl cyanide. *Mol. Phys.* **1984**, *51*, 1141–1161.

(8) Cammarata, M.; Lorenc, M.; Kim, T. K.; Lee, J. H.; Kong, Q. Y.; Pontecorvo, E.; Lo Russo, M.; Schiró, G.; Cupane, A.; Wulff, M.; Ihee, H. Impulsive solvent heating probed by picosecond x-ray diffraction. *J. Chem. Phys.* **2006**, *124*, 124504.

(9) Ihee, H.; Wulff, M.; Kim, J.; Adachi, S. Ultrafast x-ray scattering: Structural dynamics from diatomic to protein molecules. *Int. Rev. Phys. Chem.* **2010**, *29*, 453–520.

(10) Kim, T. K.; Lee, J. H.; Wulff, M.; Kong, Q.; Ihee, H. Spatiotemporal kinetics in solution studied by time-resolved x-ray liquidography (solution scattering). *ChemPhysChem* **2009**, *10*, 1958–1980.

(11) Ki, H.; Oang, K. Y.; Kim, J.; Ihee, H. Ultrafast x-ray crystallography and liquidography. *Annu. Rev. Phys. Chem.* **2017**, *68*, 473–497.

(12) Chen, X.; Ma, C.; Kwok, W. M.; Guan, X.; Du, Y.; Phillips, D. L. A Theoretical investigation of *p*-hydroxyphenacyl caged phototrigger compounds: How water induces

the photodeprotection and subsequent rearrangement reactions. *J. Phys. Chem. B* **2007**, *111*, 11832–11842.

(13) Givens, R. S.; Heger, D.; Hellrung, B.; Kamdzhilov, Y.; Mac, M.; Conrad, P. G.; Cope, E.; Lee, J. I.; Mata-Segreda, J. F.; Schowen, R. L.; Wirz, J. The photo-Favorskii reaction of *p*-hydroxyphenacyl compounds is initiated by water-assisted, adiabatic extrusion of a triplet biradical. *J. Am. Chem. Soc.* **2008**, *130*, 3307–3309.

(14) Cao, Q.; Guan, X.; George, M. W.; Phillips, D. L.; Ma, C.; Kwok, W. M.; Li, M.; Du, Y.; Sun, X.-Z.; Xue, J. Ultrafast time-resolved transient infrared and resonance Raman spectroscopic study of the photo-deprotection and rearrangement reactions of *p*-hydroxyphenacyl caged phosphates. *Faraday Discuss.* **2010**, *145*, 171–183.

(15) Klán, P.; Šolomek, T.; Bochet, C.; Blanc, A.; Givens, R. S.; Rubina, M.; Popik, V.; Kostikov, A. P.; Wirz, J. Photoremovable protecting groups in chemistry and biology: Reaction mechanisms and efficacy. *Chem. Rev.* **2013**, *113*, 119–191.

(16) Frisch, M. J.; Trucks, G. W.; Schlegel, H. B.; Scuseria, G. E.; Robb, M. A.; Cheeseman, J. R.; Scalmani, G.; Barone, V.; Petersson, G. A.; Nakatsuji, H.; Li, X.; Caricato, M.; Marenich, A. V.; Bloino, J.; Janesko, B. G.; Gomperts, R.; Mennucci, B.; Hratchian, H. P.; Ortiz, J. V.; Izmaylov, A. F.; Sonnenberg, J. L.; Williams; Ding, F.; Lipparini, F.; Egidi, F.; Goings, J.; Peng, B.; Petrone, A.; Henderson, T.; Ranasinghe, D.; Zakrzewski, V. G.; Gao, J.; Rega, N.; Zheng, G.; Liang, W.; Hada, M.; Ehara, M.; Toyota, K.; Fukuda, R.; Hasegawa, J.; Ishida, M.; Nakajima, T.; Honda, Y.; Kitao, O.; Nakai, H.; Vreven, T.; Throssell, K.; Montgomery Jr., J. A.; Peralta, J. E.; Ogliaro, F.; Bearpark, M. J.; Heyd, J. J.; Brothers, E. N.; Kudin, K. N.; Staroverov, V. N.; Keith, T. A.; Kobayashi, R.; Normand, J.; Raghavachari, K.; Rendell, A. P.; Burant, J. C.; Iyengar, S. S.; Tomasi, J.; Cossi, M.; Millam, J. M.; Klene, M.; Adamo, C.; Cammi, R.; Ochterski, J. W.; Martin, R. L.; Morokuma, K.; Farkas, O.; Foresman, J. B.; Fox, D. J. Gaussian 16 Rev. C.01, **2016**.